Assessment of the durability of various cementitious materials subjected to low levels of H2S in wastewater networks

Janette Ayoub, Marielle Guéguen-Minerbe, Tony Pons, Marcos Oliveira, Sabrina Guérin-Rechdaoui, Mario Marchetti

Metadata of the article that will be visualized in OnlineFirst

ArticleTitle	Assessment of the durability of various cementitious materials subjected to low levels of H_2S in wastewater networks	
Article Sub-Title		
Article CopyRight	The Author(s), under exclusive licence to RILEM (This will be the copyright line in the final PDF)	
Journal Name	Materials and Structures	
Corresponding Author	FamilyName	**Ayoub**
	Particle	
	Given Name	**Janette**
	Suffix	
	Division	MAST-CPDM
	Organization	University Gustave Eiffel
	Address	Marne-La-Vallée, 77454, Paris, France
	Phone	
	Fax	
	Email	janette.ayoub@univ-eiffel.fr
	URL	
	ORCID	http://orcid.org/0009-0005-4045-6058
Author	FamilyName	**Minerbe**
	Particle	
	Given Name	**Marielle Guéguen**
	Suffix	
	Division	MAST-CPDM
	Organization	University Gustave Eiffel
	Address	Marne-La-Vallée, 77454, Paris, France
	Phone	
	Fax	
	Email	marielle.gueguen@univ-eiffel.fr
	URL	
	ORCID	
Author	FamilyName	**Pons**
	Particle	
	Given Name	**Tony**
	Suffix	
	Division	MAST-CPDM
	Organization	University Gustave Eiffel
	Address	Marne-La-Vallée, 77454, Paris, France
	Phone	
	Fax	
	Email	tony.pons@univ-eiffel.fr
	URL	
	ORCID	
Author	FamilyName	**Oliveira**
	Particle	
	Given Name	**Marcos**
	Suffix	
	Division	
	Organization	SIAAP- Direction Innovation
	Address	82 Avenue Kléber, 92700, Colombes, France
	Phone	
	Fax	
	Email	marcos.oliveira@siaap.fr
	URL	
	ORCID	

Author	FamilyName	**Guérin-Rechdaoui**
	Particle	
	Given Name	**Sabrina**
	Suffix	
	Division	
	Organization	SIAAP- Direction Innovation
	Address	82 Avenue Kléber, 92700, Colombes, France
	Phone	
	Fax	
	Email	sabrina.guerin@siaap.fr
	URL	
	ORCID	
Author	FamilyName	**Marchetti**
	Particle	
	Given Name	**Mario**
	Suffix	
	Division	MAST-UMR MCD
	Organization	University Gustave Eiffel-Cerema
	Address	Marne-La-Vallée, 77454, Paris, France
	Phone	
	Fax	
	Email	mario.marchetti@univ-eiffel.fr
	URL	
	ORCID	

Schedule	Received	8 Dec 2023
	Revised	
	Accepted	28 Mar 2024

Abstract	Wastewater networks are intrinsically attacked by the production of H_2S, a highly reactive gas known for its extremely aggressive nature. This study employs a range of techniques, such as XRD, SEM–EDS, TGA, and Raman spectrometry, to investigate the interaction between low concentrations of H_2S—averaging 1.3 ppm and various types of Portland cementitious materials (CEM I, CEM II, CEM III, and CEM V). The objective is to discern the chemical alterations contributing to structural deterioration and to provide a mineralogical characterization of the deterioration layers present on these binders.

Keywords (separated by '-')	Biodeterioration - Cementitious materials - Low H_2S concentration - Durability - SEM–EDS - μ-Raman
Footnote Information	

Materials and Structures _####################_
https://doi.org/10.1617/s11527-024-02346-6

ORIGINAL ARTICLE

Assessment of the durability of various cementitious materials subjected to low levels of H_2S in wastewater networks

Janette Ayoub · Marielle Guéguen Minerbe · Tony Pons · Marcos Oliveira · Sabrina Guérin-Rechdaoui · Mario Marchetti

Received: 8 December 2023 / Accepted: 28 March 2024

Abstract Wastewater networks are intrinsically attacked by the production of H_2S, a highly reactive gas known for its extremely aggressive nature. This study employs a range of techniques, such as XRD, SEM–EDS, TGA, and Raman spectrometry, to investigate the interaction between low concentrations of H_2S—averaging 1.3 ppm and various types of Portland cementitious materials (CEM I, CEM II, CEM III, and CEM V). The objective is to discern the chemical alterations contributing to structural deterioration and to provide a mineralogical characterization of the deterioration layers present on these binders. Through a comprehensive examination of the durability of these materials exposed to low concentrations of H_2S in a Paris Region sewage system over nearly four years, the findings extend beyond surface-level observations. Despite the absence of visible signs of deterioration, high-precision analytical techniques reveal significant mineralogical transformations within the cementitious matrix. Expansive products such as gypsum, ettringite, and elemental sulfur are identified in mortar samples, underscoring the critical role of precise analysis in comprehending the deterioration process.

Keywords Biodeterioration · Cementitious materials · Low H_2S concentration · Durability · SEM–EDS · μ-Raman

J. Ayoub (✉) · M. G. Minerbe · T. Pons
MAST-CPDM, University Gustave Eiffel,
Marne-La-Vallée, 77454 Paris, France
e-mail: janette.ayoub@univ-eiffel.fr

M. G. Minerbe
e-mail: marielle.gueguen@univ-eiffel.fr

T. Pons
e-mail: tony.pons@univ-eiffel.fr

M. Oliveira · S. Guérin-Rechdaoui
SIAAP- Direction Innovation, 82 Avenue Kléber,
92700 Colombes, France
e-mail: marcos.oliveira@siaap.fr

S. Guérin-Rechdaoui
e-mail: sabrina.guerin@siaap.fr

M. Marchetti
MAST-UMR MCD, University Gustave Eiffel-Cerema,
Marne-La-Vallée, 77454 Paris, France
e-mail: mario.marchetti@univ-eiffel.fr

1 Introduction

Underneath the dynamic urban landscape lies a complex and often overlooked sewer system network that silently plays a crucial part in ensuring public health and environmental sustainability. Cementitious materials, which form the backbone of the sewer network, are at the root of the success of these underground pipes. These materials are a key to ensuring the sewer infrastructure's structural integrity, durability, and overall efficiency.

Indeed, throughout their lifespan, these pipes encounter a range of deterioration processes, which

can arise from assembly defects, environmental constraints, or deterioration triggered by the presence of substances and microorganisms within the pipe. Thus, in about 40% of cases, this damage can be linked to a biogenic attack resulting from sulfuric acid production [1]. This particular mode of deterioration, encountered in concrete structures subjected to sewage environments, has the potential to substantially reduce the lifespan of these structures [2, 3]. For instance, it can diminish the 100-year expected service life to a range of 30–50 years, or even, in the most severe cases, to 10 years or less [3, 4].

The phenomenon of microbiologically induced acid deterioration in concrete has garnered significant attention since its identification. The sequence of stages that initiate and advance concrete biodeterioration in sewage environments has been delimited into several steps by various researchers [3, 5–11]. However, the most commonly agreed-upon sequences can be summarized as previously schematized by Herisson et al. [12]. This process begins with the creation of anaerobic zones at the bottom of pipes by wastewater sediments. In these specific zones, the low concentration of oxygen leads sulfate-reducing bacteria (SRB) to reduce sulfur compounds, such as sulfates, into highly volatile hydrogen sulfide (H_2S). Subsequently, depending on the network's temperature, pH, hydrodynamics, and the concentration of oxidized sulfur compounds in the wastewater, H_2S volatilizes into the pipe atmosphere above the water flow. Gaseous H_2S condenses on the pipe surface and affects the cementitious matrix in two distinct yet interconnected ways. The first of these pathways acts directly by reducing the surface pH of cementitious materials, resulting in immediate effects. Nevertheless, it's important to note that, at this stage, the pH cannot attain an acidic value. However, the second, more complex path involves a fascinating chain of four key stages: the initial abiotic conversion of H_2S into sulfur components on the surface of the cementitious material; the subsequent bacterial oxidation of sulfur compounds into sulfuric acid; the diffusion of sulfuric acid into the cementitious matrix; and ultimately the gypsum formation.

The biodeterioration of sewage cementitious matrices has attracted considerable global research attention, with notable studies in occidental countries such as Australia, Austria, France, Germany, Denmark, and the United States among others [6–8, 10, 13]. However, among these studies, the H_2S levels investigated consistently reached high concentrations, which often exceeded 600 ppm, leaving a gap in research into low H_2S concentrations. Consequently, the ability of sewage cementitious materials to withstand low H_2S environmental conditions remains under-explored.

This study addresses this gap by investigating the performance and durability of various Portland cementitious materials (CEM I, CEM II, CEM III, and CEM V) under low H_2S concentrations exposure. Additionally, it provides a mineralogical characterization of deterioration layers found on these binders. Understanding the processes in the cementitious matrix at low H_2S concentrations is crucial for implementing effective prevention and maintenance procedures, ensuring the long-term durability and performance of vital infrastructure in wastewater networks.

Accordingly, different mortar formulations were exposed in situ for a period of nearly 4 years in a sewage system, with periodic macroscopic monitoring. Various analytical techniques found application in this study, such as X-ray diffraction (XRD), scanning electron microscopy equipped with an energy-dispersive X-ray spectrometer (SEM–EDS), and thermogravimetric analysis (TGA). Furthermore, by leveraging this wide range of practical instrument configurations, Raman spectrometry outperforms other methods with its diverse advantages [14, 15]. This technique is nowadays widely applied to characterize civil engineering materials and continuously assess their evolution throughout their life cycle, from initial anhydrous materials to hydrated and hydrating pastes, and all the way to their degraded state [16–18].

2 Materials and experimental approaches

2.1 Mortar samples

These mixtures were established to be representative of the real-world sewer network to assess their resistance to deterioration.

The mortar specimens used in this study were prepared with four different types of cement: ordinary Portland cement (CEM I), Portland-composite cement (CEM II), blast furnace cement (CEM III), and composite cement (CEM V). Three specimens

were prepared for each type of cement. In all mixtures, the water-to-cement ratio was 0.5 and the sand-to-cement ratio was 3. The mortars were molded into cylinders with a 6 cm diameter and a 12 cm height. A PVC tube was also precisely inserted into the central portion of each sample to ease their handling.

Once formed, the specimens were exposed to a 100% relative humidity atmosphere over 24 h, then unmolded and stored in sealed plastic bags for a curing period of 28 days. Then, they were placed inside a $60\times40\times30$ cm^3 compartment that was afterward installed inside the sewer network and exposed to the specific sewer gas flow. Figures 1 and 2 in Herisson et al.'s [12] study provide a clear understanding of the appearance and placement of the specimens on site.

2.2 Exposure site of mortar samples

The northern part of the greater Paris Sanitation Authority (SIAAP in French), has been selected as a suitable exposure site for the 44 months study period. In addition to stormwater and industrial wastewater, SIAAP carries and purifies the wastewater of nine million residents within and around Paris, enhancing the dynamic natural environments of the Seine and Marne rivers. The selected site has been chosen based on precise previous results showing that the area exhibited relatively low H_2S concentrations.

OdaLog® safety sensors were inserted alongside the samples in the compartment in order to track the concentration of H_2S and temperature throughout the study period. Figure 3 and Table 1 present a 9-month example of the results obtained from these sensors used to assess the environmental conditions. During this period, the site recorded an average H_2S concentration of 1.3 ppm, which categorizes it as a moderately chemically aggressive environment according to the NF EN 206/CN [19], designated as XA2.

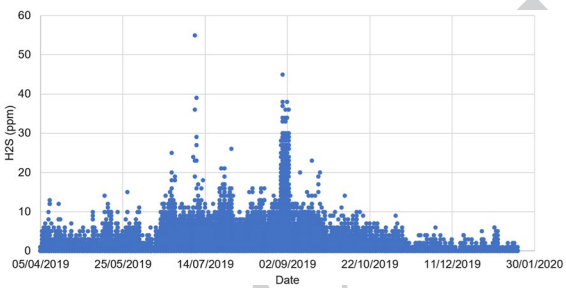

Fig. 1 H_2S concentration versus Time over 9 months at the SIAAP facility

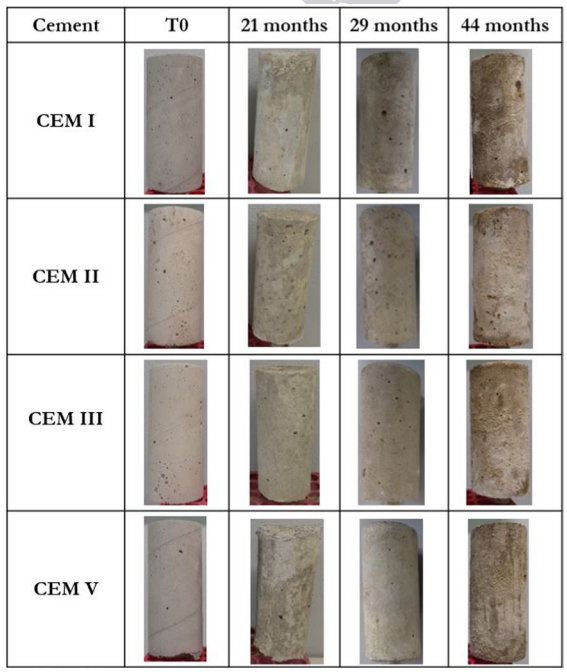

Fig. 3 In-situ visual evolution of mortar samples exposed over 44 months at a low H_2S concentration

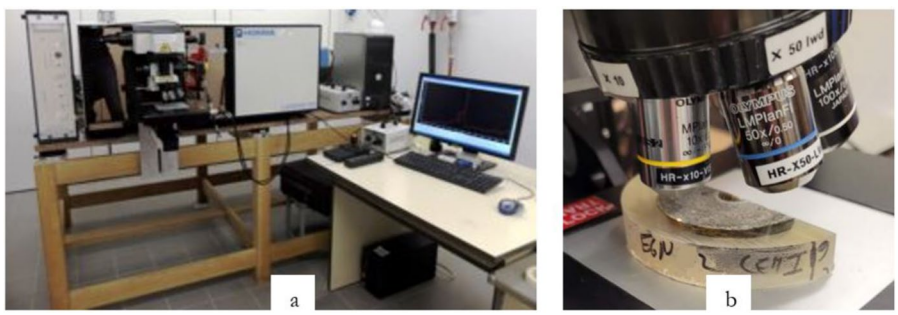

Fig. 2 LabRam HR800 (**a**) and CEM I sample before 2D mapping (**b**)

Table 1 Overview of H_2S concentration (ppm) data over 9 months of the study period

Mean	Standard deviation	1st quartile	3rd quartile	Minimum	Maximum
1.3	2.7	0.0	1.0	0.0	55.0

Moreover, as detailed in Table 1, the data shows that the first quartile stands at 0.0 ppm, representing the lower 25% of the measured concentrations, while the third quartile is at 1.0 ppm, signifying the value below which 75% of the data falls. The computed values presented in Table 1 provide a comprehensive view of the distribution of H_2S concentrations, which, in turn, reveals that the specimens were not exposed to a severe H_2S environment with respect to this gas.

2.3 Testing procedure

2.3.1 In-situ evolution monitoring

At each sampling time step (21, 29, and 44 months after exposure), in situ photographs of the specimens were captured to document the macroscopic degradation of the specimens over time. Additionally, the weights of the mortars (measured with a scale accurate to 0.1 g), surface pH (determined using pH paper with a precision of 0.2), and diameters (measured with a caliper) were recorded to monitor changes in the properties over time.

After a 44-month exposure period in the sewage network, the mortars were carefully collected from their cases and accurately processed to secure consistent test conditions and results. The specimens were then entirely covered with epoxy resin (EpoFix, Struers) under vacuum conditions to preserve the deterioration condition. This precaution was taken to ensure the sample's structural integrity for further testing.

Before all the analysis, the mortars exposed in-situ for 44 months underwent a meticulous diamond polishing process with ethanol that yielded homogeneous and plane test surfaces.

2.3.2 Scanning electron microscopy with energy dispersive x-ray spectrometer (SEM–EDS)

Analyses were carried out using a Scanning electron Microscope (Quanta 400 FEI) equipped with an Energy Dispersive X-ray Spectrometer (EDS, Xplore30, Oxford), operating at an acceleration voltage of 20 kV. After carbon metallization of the polished surface, a panorama was acquired using backscattered electrons in order to identify deteriorated areas. Maps were acquired using the intensity of the Kα rays for the relevant chemical elements (Si, Ca, Mg, K), modifications being expected after the attack for these specific ones.

2.3.3 X-ray diffraction (XRD) analyses

In order to detect and identify the crystalline phases present and their possible in-core degree of penetration, three holes were drilled at three successive distances, from the sample's edge to its center, using 3 mm diameter drills, as shown in Fig. 8 of Appendix 1 . Subsequently, the resulting cement powder was gathered for qualitative analysis by X-ray diffraction (XRD). The XRD measurements were performed using a PANalytical Empyrean diffractometer equipped with Co Kα radiation and a PIXcel^{3D} detector. Current and voltage on the X-ray tube were 30 mA and 40 kV, respectively. The diffractograms were acquired in the range of 2θ from 4° to 76° with a step size of 0.013° 2θ/s. Mineral identification was carried out using the HighScore Plus software with the crystallography open database (COD) [20–27].

2.3.4 Thermogravimetric analysis (TGA—DTA) coupled with a mass spectrometer

Using the resulting cement powder gathered from the drilling process described in the subSect. 2.3.3., the thermogravimetric (TGA) and differential thermal (DTA) analysis for the identification of the different phases, progressing from the edge of the sample towards its center, was carried out in a dry argon atmosphere using a NETZSCH STA 409E simultaneous thermal analyzer, performing both TGA and DTA simultaneously. The selected temperature ramp was 30–1250 °C, with an argon flow rate of 40 ml/min and a heating rate of 10 °C/min. All through the heating process, weight changes are generated by the loss of H_2O and CO_2 as the temperature increases. Emitted gas, H_2O, and CO_2 were monitored over time using a mass spectrometer, with 18.09 g/mol, and 44.09 g/mol respectively used as molar masses.

2.3.5 μ-Raman spectroscopy

As shortly mentioned in the introduction, Raman spectroscopy is now implemented in the characterization of civil engineering materials, and in the continuous monitoring of some of their evolution. In addition to all the advantages that Raman spectroscopy offers, such as being a non-destructive and rapid technique, it has been found to successfully detect the sulfate attack product in cementitious materials [28, 29].

Precise punctual measurements were conducted along a radial line over a section of the samples (cf. Figure 9 of Appendix 1) to enhance the investigation of the mineralogical characterizations of the mortar samples. The analyses were performed using two different instruments.

The first one was a BWTek iRaman spectrometer operating with a 532 nm laser wavelength and delivering nearly 50 mW power output. The 2048-pixel CCD detector provided spectra over the 150–4000 cm^{-1} spectral range with a resolution of 4 cm^{-1}. It was paired to a BAC151C microscope, and spectral measurements were made through an×50 objective lens from Olympus. Both BWTek instruments are managed by BWSpec 4.11_1 software.

The second spectrometer was a LabRAM HR800 spectrometer operating with a 514 nm laser wavelength and delivering nearly 1 mW power output. The instrument is optically coupled to a BX-model microscope from Olympus, with a×50 (NA 0.75) MPlanN objective. The diffraction-limited spot size is then about 1 μm. The detector provided spectra over the 50–4000 cm^{-1} spectral range with a resolution of 1 cm^{-1}. An XY-motorized stage allowed to taking of in-line profiles and 2D mappings with a displacement step as low as 1 μm. All devices are controlled by LabSpec 6 software.

3 Results

3.1 In situ visual evolution monitoring

Photographs taken at each time scale provided an overview of a qualitative visual evolution of the cementitious materials, as shown in Fig. 3. Since the very first sampling period (21 months), the deterioration of all the specimens has been observed and has evolved over the years. Indeed, according to the literature with samples exposed to average H_2S concentrations of 5 and 100 ppm respectively [30, 31], samples were expected to show much more noticeable visual deterioration after 44 months of exposure. Therefore, it can be noticed that the mortars are moderately well preserved and that this limitation of degradation can be strongly linked to their exposure to a very low concentration of H_2S.

Based on the visual characteristics only, throughout the study period, the changes in all samples were characterized by the presence of white crystals and brownish deposits. At the end of the 44 months, the specimens had somewhat darkened and showed some deterioration marks, notably the growth of expansive products.

Alongside a visual inspection of the degradation, sample weights were measured during the *in-situ* exposure period. All the examined mortars exhibited identical behavior, as illustrated in Fig. 4. Over the first 21 months, a weight gain is recorded, which can be linked to the accumulation of water in the pores of the mortar specimens and the formation of sulfide reaction products, followed by a slight weight loss. It is crucial to highlight that all the types of cement used in the study showed a similar variation in weight percentage.

The examination of pH values throughout the study period revealed a significant drop in the surface pH, from its initial alkaline value to an acidic value after 21 months, followed by stabilization in the 4–6 range over the subsequent months. This pattern reflects the results documented in existing literature [30–32].

Furthermore, the investigation of the diameter evolution over the 44 months did not reveal any

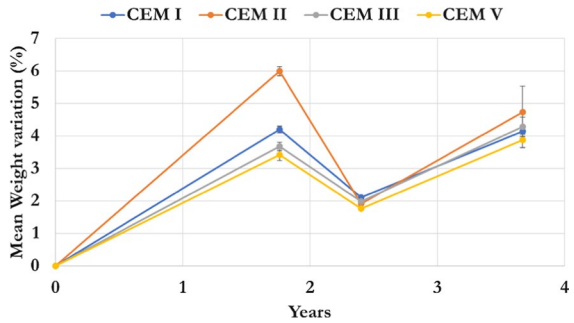

Fig. 4 Mean weight variation of mortar samples exposed for 44 months at a low H_2S concentration

significant change for all the specimens. The percent change in diameter ranged from 0 to 0.7% of expansion over the study period, which is consisted with the visual observations that did not reveal any noticeable expansion of the mortars.

3.2 Chemical profile maps determination

SEM observations and elemental map investigations facilitated the identification of diverse elemental chemical distributions and sample zonation. Figures 10–13 in the Appendix illustrate the multimodal analysis of the mortar specimens, presenting visualizations of cross-sections obtained using KEYENCE, SEM imaging of half the section and the selected section to be analyzed with EDS. The interpretation of chemical variations relied on the distribution of elements compounds determined through EDS analysis. The identification of various microstructural zones in all examined deteriorated mortar samples closely aligns with previous findings [32–35]. Furthermore, a consistent behavior was observed across all samples, attributed to their shared composition of Portland cement. This emphasizes the reliability of the results and underscores a uniform response to selected environmental factors.

Four distinct zones have been distinguished in these samples through meticulous analysis, as illustrated in Figs. 5 and 6. Each zone reveals unique features indicating specific compositional, mineralogical, and microstructural characteristics.

The first zone, prominently visible in the SEM images, consisted of a strongly altered area. This near-surface zone is locally enriched in sulfur and calcium (cf. zone 1 in Fig. 5), precipitating mainly along long reticulated crack systems.

Moving on to a second zone, its composition differed notably from the first, with a porous structure characterized by the presence of Si and the depletion of the S and Ca elements, creating a distinctive void in the elemental composition. Additionally, this zone is characterized by the absence of anhydrous phases (such as C2S, C3S, etc.). In the backscatter images, anhydrous phases typically appear as white elements; however, they are absent in this specific zone of the section. This particular zone can be most precisely described as an outer transition zone, representing a boundary between the strongly deteriorated external zone and the slightly deteriorated internal zone.

The third zone can be most accurately described as an inner transition zone, marked by the accumulation of K and Mg elements, followed by the successive incorporation of S and Ca. Furthermore, this zone can be subdivided into two distinct inter zones, labeled 3a and 3b. These sub-zones are clearly differentiated by the absence of anhydrous phases in zone 3a and their presence in zone 3b, with an additional layer of complexity to the mineralogical composition in this transitional region. This zone further contributes to the comprehensive understanding of the sample's heterogeneity.

These deteriorated layers probably consist of newly formed calcium sulfates. These layers are identified by regions where calcium and sulfur have accumulated. Additionally, they are less defined layers containing silicon. However, in cases where only sulfur was detected in the elemental distribution images, the presence of elemental sulfur was probable.

Lastly, a fourth zone, which can be described as the pristine zone, indicates that its mineralogical composition has remained relatively unchanged. This zone features an abundance of anhydrous phases (such as C2S, C3S, slag, …) identifiable on BSE images. The presence of anhydrous phases indicates a chemical reaction of the water with the initial cement, potentially contributing to the zone's resistance to the deleterious effects of H_2S. Indeed, the distinction between all the zones can be effectively discerned through the variations in texture from one zone to its neighbors.

From the results illustrated in Fig. 5, the CEM I sample features all four of the identified zones. On the other hand, the CEM III and CEM V samples exhibit similar zonation, whereby the second zone is notably lacking. Conversely, the CEM II sample presents a marked change in element distribution, as illustrated in Fig. 6. Particularly in its third zone, where the element sulfur is notably absent.

With these findings and ImageJ software [36], measurements of minimum and maximum values were taken for each zone of the samples for comparative analysis, as shown in Table 1. The results reveal that all the samples present deteriorated layers in varying degrees of proximity. Remarkably, AQ4 the CEM II sample was found to be the most deteriorated of all the Portland cement samples studied (Table 2).

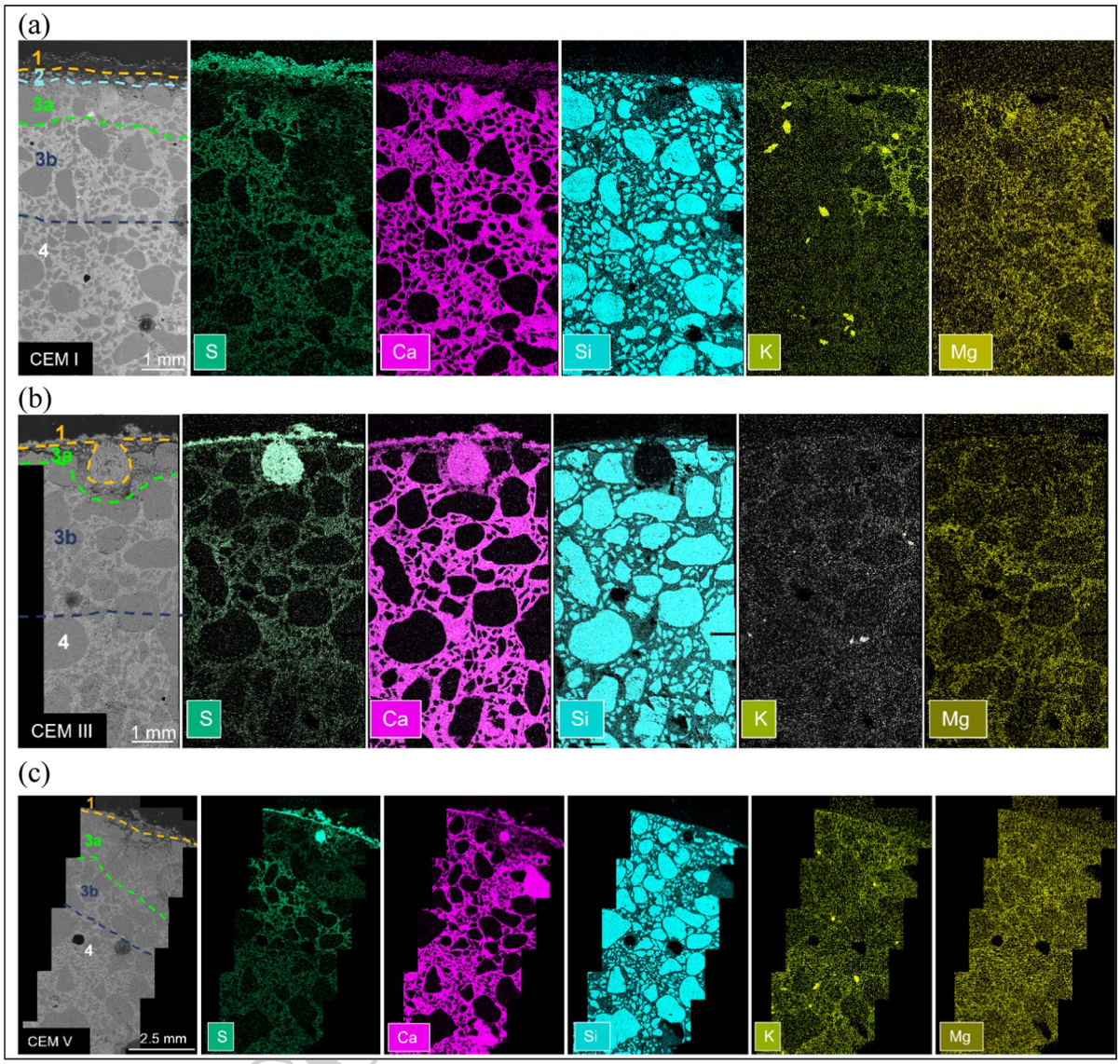

Fig. 5 High resolution and elemental distribution images of S, Ca, Si, K, and Mg of cross-sections in **a** CEM I, **b** CEM III, and **c** CEM V samples, revealing the varied zones from the exterior deteriorated zone to the interior pristine zone

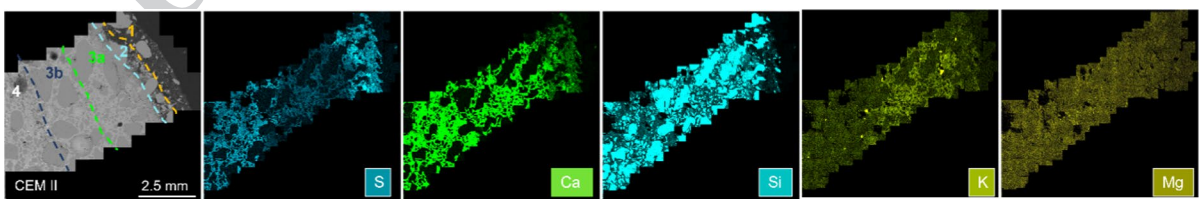

Fig. 6 High resolution and elemental distribution images of S, Ca, Si, K, and Mg of cross-sections in the CEM II sample, revealing the varied zones from the exterior deteriorated zone to the interior pristine zone

Table 2 Alteration zone thickness variations for various cement types in mm (min–max)

	Zone 1	Zone 2	Zone 3a	Zone 3b
CEM I	0.2–0.5	0.2–0.3	0.9–1.1	1.9–2.3
CEM II	0.8–1.4	0.6–0.7	1.7–2.1	1.7–2.4
CEM III	0.3–0.9	NA	0.2–0.3	2.623.2
CEM V	0.2–0.7	NA	1.9–2.1	1.9 –2.1

3.3 Mineralogical characterization

XRD (X-ray Diffraction) and TGA (Thermogravimetric Analysis), analyses were carried out for the mineralogical characterization of the cementitious samples into the depth of the materials constituting the samples. Nevertheless, considering the information presented in Sect. 3.2 and the fact that the holes in the samples were obtained using 3 mm drills, it can be asserted that the first hole falls within the three predefined zones. Consequently, differentiation of results based on specific zones, according to XRD and TGA, is not feasible. However, it can be considered that the first hole occurred in the deteriorated part of the sample (zones 1, 2, 3a, and 3b previously described in Sect. 3.2 and shown in Figs. 5 and 6), while the other two occurred in the intact zone (zone 4 previously described in Sect. 3.2.).

Qualitative XRD analyses of the resulting cement powder showed the quartz (peak at 3.34 Å) contained in the sand to be the main crystallized phase for all the holes of the four cement types.

For the Ordinary Portland cement sample CEM I, XRD results revealed the presence of the semi-hydrated phase of gypsum 'bassanite' ($CaSO_4 \cdot 0.5H_2O$, peak at 3.00 Å) and calcite ($CaCO_3$, peak at 3.04 Å), in the altered layer of the sample indicating the local variation in the mineralogical composition of the sample due to the biogenic H_2S attack. Furthermore, portlandite (peak at 2.63 Å) was detected throughout the core of the sample. Figure 14 of Appendix 1 shows the diagrams of the three holes of the CEM I specimen.

For the CEM II and CEM III samples, XRD analyses confirmed the predominance of quartz, but other phases such as calcite and portlandite were also identified throughout the radial line of the samples. Moreover, vaterite (peak at 3.29 Å) was also detected in the CEM III sample.

Nevertheless, for the CEM V sample, no other phases apart from quartz were detected in the intact zone of the sample. However, in the deteriorated zone, gypsum (peaks at 7.62 and 4.27 Å) and calcite were identified.

On the other side, the TGA-MS results for all the samples revealed the presence of four distinctive stages of weight loss over the entire temperature range, spanning from 30 to 1250 °C.

The initial weight loss, occurring between room temperature and 220 °C, was attributed to the evaporation of all free water and of water from the C–S–H and ettringite components. The following weight loss, between 380 and 500 °C, is mainly due to the liberation of water during the dehydration process of portlandite. This percentage weight loss can be effectively used to estimate the portlandite content of samples. With the third stage of weight loss, which takes place between 700 and 800 °C, CO_2 is released, making it possible to estimate the $CaCO_3$ content in the mortar samples. The final weight loss observed above 1000 °C is attributed to the release of SO_3, which originates from the sulfates contained in the gypsum and ettringite due to the H_2S attack in the mortar samples [9].

Taking all the findings together, it is confirmed that the samples have undergone an alteration with a mineralogical modification. However, it should be noted that this change was not as severe as that previously recorded for samples heavily exposed to H_2S [8–10, 37]. The mineral phases identified in the samples of this study suggest alteration, but to a lesser degree, underlining the importance of environmental conditions in the mineral alteration process.

Moreover, these results demonstrate that after 44 months of in-situ exposure in a sewer environment, all Portland cement-based mortars contain portlandite all over the different zones of the samples. This finding can be justified by the low concentration of H_2S in the exposition zone, as the reduced presence of hydrogen sulfide leads to a less aggressive chemical environment.

3.4 Mineralogical characterization by micro-Raman spectroscopy

Among the different methods assessed, the Raman spectroscopy analysis consistently identified the presence of gypsum in the deteriorated layers of all

the specimens under investigation. Notably, gypsum formation is characteristic of the sulfate attack of a cementitious material. This material has a specific peak at 1003 cm^{-1}, as indicated in the literature [38].A photograph of an altered zone of a polished section of the exposed CEM V sample is shown in Fig. 7a. Additionally, Fig. 7b presents its spectral analysis over two spectral ranges (laser at 514 nm, 25-s acquisition time, and averaged over 4 spectra), with an emphasis on the intensification characteristic of the gypsum spectrum. It is crucial to outline that the observed vibrational modes closely align with the literature data [29, 37, 39, 40].

Starting with the CEM I specimen exposed to the H_2S-enriched environment, alongside gypsum, the analysis revealed the presence of ettringite and two calcium carbonate polymorphs (calcite and vaterite, with a main intense peak respectively at 1085 cm^{-1} and 1077–1090 cm^{-1}) [29, 41–43]. Ettringite and gypsum were detected in the altered zone, and according to the literature, they have been identified as the main reason for the sulfate attack damage [29, 44]. However, calcium carbonate was detected along the radial line of the sample.

Moving on to the CEM II specimen, calcite was identified in all the measurements taken, indicating its consistent presence. The existence of this supplementary phase within the alteration layer suggests that the formation of gypsum might have arisen either from calcium ions present in the constituent phases of the cementitious matrix (portlandite and C–S–H) or from calcite. Moreover, it is worth noting that calcite is consistently observed in all the samples and at greater depths within the mortars. The presence of $CaCO_3$ in the samples' sections could also be attributed to an unavailable carbonation occurring once the inner part of the samples had been exposed to the atmosphere and during the polishing process, despite cautious storage conditions.

For the CEM III sample, the sulfite mineral hannebachite was also detected at the surface of the mortar sample [45]. As per prior studies, Pons et al. [37] also identified hannebachite in a previous CEM III mortar sample.

Lastly, in the case of the CEM V specimen, ettringite and calcite were also detected in addition to gypsum.

All these findings reinforce the spectroscopic technique's importance for assessing the cementitious matrix's bio-alteration, but also about its spatial resolution with respect to TGA and XRD.

4 Discussion

This study highlights the significant synergies arising from the utilization of diverse analytical techniques. While each method provided valuable data independently, the true strength of the results emerged when considering the correlations and relationships revealed through their collective examination. The interconnections observed among XRD, SEM–EDS, TGA-MS, μ-Raman spectroscopy, and in situ monitoring collectively present a comprehensive portrayal of the impact of low H_2S concentrations on cementitious materials in sewage systems. These techniques, when integrated, offer a holistic view, uncovering mineralogical modifications and chemical alterations

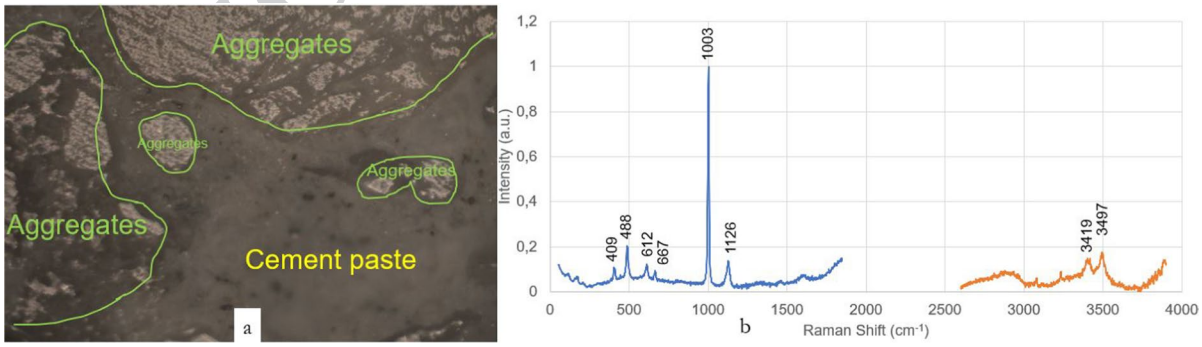

Fig. 7 **a** Photograph in reflected light of a CEM V altered zone, and **b** a normalized Raman spectrum (obtained with the LabRAM HR800 spectrometer) after 44 months of exposure in a sewage system

within the cementitious matrix. This multifaceted approach proves crucial, as it goes beyond the limitations of any single analytical method.

The intricate nuances of material degradation in cement samples exposed to an H_2S-enriched atmosphere in wastewater networks are brought to light through meticulous scanning electron microscopy observations. The SEM reveals a fascinating diversity within the deteriorated portions of the sample, where different zones, each characterized by distinct chemical features and sizes, emerge even in the thinnest sections. This microscale analysis, with its capacity to discern minute variations, surpasses the capabilities of traditional tools such as TGA and XRD. The revelation of specific characteristics within each zone, despite their thinness, underscores the non-uniform nature of the degradation process. It becomes evident that a comprehensive understanding of this complex interaction necessitates a diversified analytical approach. This exploration not only highlights the limitations of singular analytical tools but emphasizes the imperative role of complementary techniques.

In this context, SEM, with its precision at the microscale, and Raman spectroscopy stand out as pivotal contributors. Their integration facilitates a more holistic analysis, providing unparalleled insights into the intricate interplay between cement samples and H_2S. This synergy between SEM and Raman spectroscopy transcends the individual constraints of each technique, offering a comprehensive understanding of the material deterioration process. In essence, this approach broadens the horizons of material science, demonstrating the indispensability of diverse analytical tools in unraveling the complexities of biodegradation in cement exposed to environmental stressors.

In this research, the analysis of element distribution in deteriorated concrete layers revealed a dynamic system influenced by pH and diffusion of elements into the cement matrix. It revealed a clear sequence of element accumulation closely linked to pH levels, the dissolution and precipitation of solids, some variations in chemical compositions of cementitious binders, and the spatial distribution of bacteria present in the wastewater.

The strongly deteriorated surface layer (zone 1) extending from 0.2 to 1.4 cm featured a composition comprising filamentous structures composed of S and Ca. These structures represented the precipitation of secondary sulfate salts, including gypsum ($CaSO_4{\cdot}2H_2O$), ettringite ($Ca_6Al_2(SO_4)_3(OH)_{12}{\cdot}26H_2O$), anhydrite ($CaSO_4$), hannebachite ($CaSO_3{\cdot}H_2O$), and bassanite ($CaSO_4{\cdot}0.5H_2O$). The formation of hannebachite and bassanite can be explained by cycles of humidification and drying, leading to fluctuating SO_4^{2-} and H_2O activities in the mortar's interstitial solutions. Si-rich layers, on the other hand, consisted of amorphous silica.

The transition zone, segmented into three distinct inter zones (Zones 2, 3a, and 3b) between strongly deteriorated and intact concrete, was bounded within a range of 3–5 mm. This led to dynamic dissolution and precipitation of individual phases, as shown by the concentrations of individual elements in Figs. 5 and 6. The interface between Zones 2 and 3 in the transition zone was characterized by a reduction in Ca concentration following acid penetration. Meanwhile, a simultaneous process of sulfate incorporation along the grain boundaries was observed, suggesting that this could be associated with the interfacial transition zone and its higher portlandite content ($Ca(OH)_2$) [46]. This resulted in the microstructural deterioration of the cement matrix through the formation of expansive sulfate phases [47]. From the very initial edge of zone 3, Mg accumulation occurred as a result of the precipitation of Mg hydroxides, such as brucite ($Mg(OH)_2$). In this process, hydroxide (OH^-) diffused from alkaline areas in the intact mortar, while diffusion of Mg ions was induced by Mg precipitation and the associated concentration gradient. Given that the stability of Mg-containing precipitates is limited to strongly alkaline conditions, the cessation of Mg precipitation marks the end of zone 3. Mg thickness and concentrations in the accumulation zone have been found to correlate directly with the dominant pH gradient, making them indicative of the rate of deterioration [33, 48]. Furthermore, in this transition zone, a noticeable accumulation of potassium (K) occurs in the elemental distribution (Figs. 5 and 6). Analysis of the compositional data suggests that these additional precipitates could be identified as (K-alum) ($KAl(SO_4)_2{\cdot}12H_2O$), syngenite ($K_2Ca(SO_4)_2{\cdot}H_2O$), or alunite ($KAl_3(SO_4)_2(OH)_6$ that is also affected by the alkaline leaching rate [33, 49].

The intact pristine zone (zone 4), identified as the inferior zone, features a matrix mainly made up of calcium- and silicon-rich phases, including portlandite and hydrated calcium silicates (C–S–H

phases) as well as anhydrous grains. This matrix envelops silica and carbonate aggregates. In addition, various calcium carbonate polymorphs, such as calcite and vaterite, have been detected in this zone.

5 Conclusion

This research has illuminated the significant impact of low H_2S concentrations on cementitious materials in sewage systems. This impact, although often overlooked, plays a fundamental role in the degradation process of the cementitious materials that constitute these systems. Previous research has focused primarily on high H_2S concentrations, yet this study unveiled the subtle but consequential effects of low H_2S levels. By combining a full range of analytical techniques, including XRD, SEM–EDS, TGA-DTA, and Raman spectroscopy, in conjunction with continuous weight measurements and visual observations, several significant breakthroughs were achieved.

On the visual side, samples subjected to low H_2S concentrations showed no dramatic indications of deterioration compared to those exposed to more harsh environmental conditions. However, the real significance of these results lies beneath the surface, since the cementitious materials underwent considerable mineralogical alterations.

Most notably, these analyses highlighted the presence of several minerals in the mortar samples, underscoring the extent of the changes observed. In particular, bassanite and hannebachite, which are precursors to gypsum and have not been identified in materials subjected to higher levels of H_2S, were discovered. Moreover, gypsum, ettringite, elemental sulfur, and various polymorphs of calcium carbonate were identified along a radial line from the edge to the core of the samples. These mineralogical transformations emphasize the complex interplay between low H_2S concentrations and the composition of cementitious materials, which, although less visible on the surface, have a considerable impact on their long-term durability.

Furthermore, magnesium and potassium were detected in the altered layers following the chemical reactions of the Portland cement-based mortars at low H_2S levels. The unexpected existence of these components underlines both the complexity and the subtlety of biogenic sulfuric attacks on cementitious materials.

Remarkably, this study showed no real difference in the durability of the various cement-based paste samples used. The absence of any significant differentiation in resistance to low H_2S concentrations suggests that there is no distinct hierarchy in the classification of pastes according to their degree of resistance. It is noteworthy, however, that the CEM II sample revealed a slightly thicker deteriorated layer than the others, pointing to a nuanced aspect in the performance of these cement pastes.

To conclude, the outcomes of this study are very consistent with the existing literature on studies at high concentrations of H_2S, highlighting the crucial importance of considering low H_2S levels when assessing the durability of cementitious matrices in wastewater systems. Moreover, this study highlights the importance of using very precise analytical techniques, such as micro-Raman and SEM–EDS, to thoroughly assess all the layers arising during the biodeterioration process.

Acknowledgements "This project has received funding from the European Union's Horizon 2020 research and innovation programme under the Marie Skłodowska-Curie COFUND grant agreement No 101034248." The authors gratefully acknowledge Gwénaël GOUADEC for his invaluable assistance in conducting several critical Raman measurements, Béatrice Desrues for her invaluable assistance in conducting the SEM-EDS acquisition, and Céline Briand for her technical assistance at SIAAP.

Funding HORIZON EUROPE Marie Sklodowska-Curie Actions, 101034248, Janette Ayoub

Data availability Data will be provided on request.

Appendix 1

See Figs. 8, 9, 10, 11, 12, 13 and 14

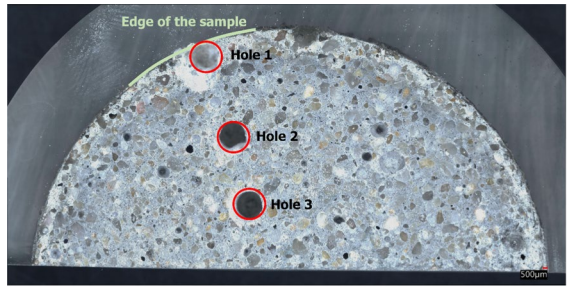

Fig. 8 A Keyence figure of a CEM V sample showing holes drilled at successive distances from the edge

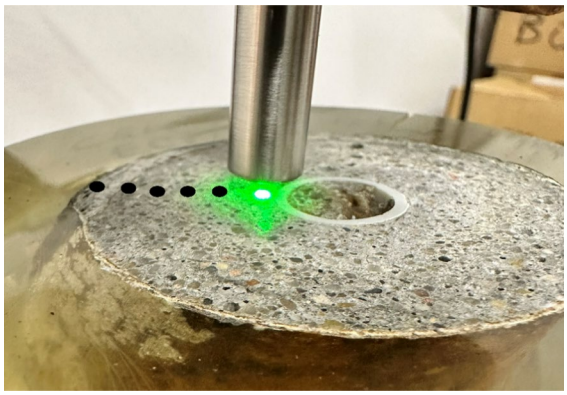

Fig. 9 Example of punctual measurements sequencing in μ-Raman spectroscopy. The green dot signifies the initial laser acquisition point, while the multiple black dots illustrate the subsequent acquisitions

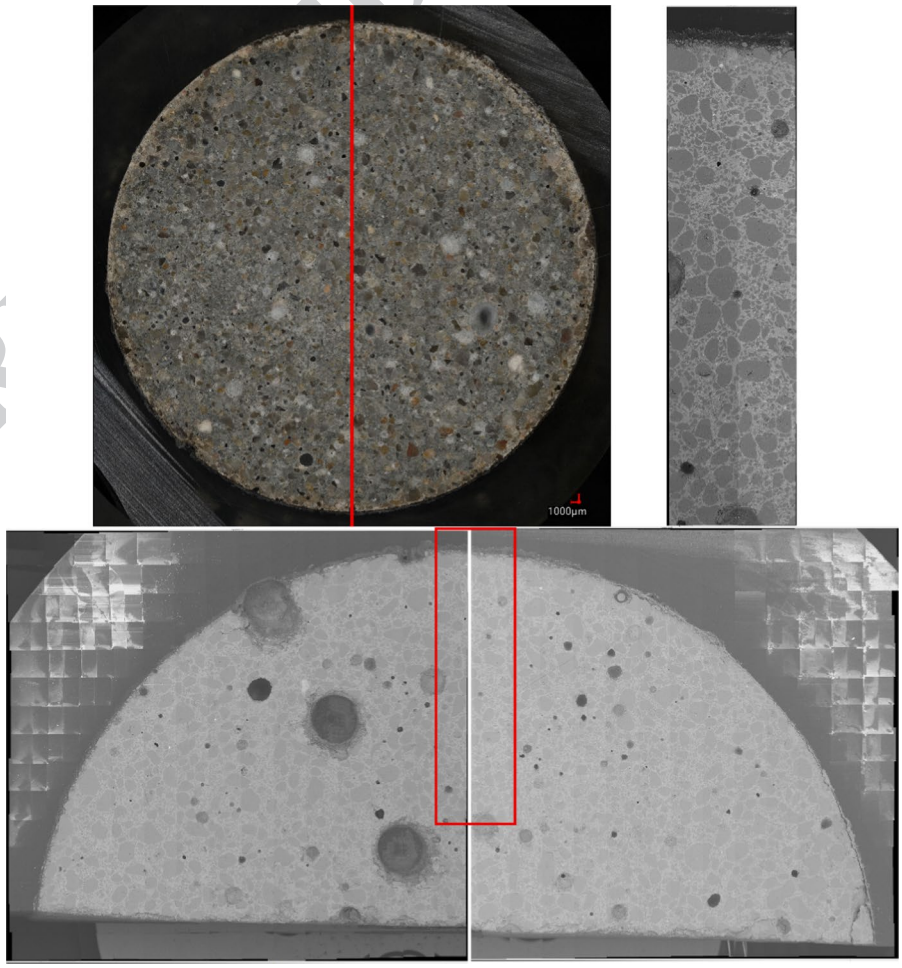

Fig. 10 Analysis of CEM I Mortar: **a** Cross section visualization with Keyence, **b** Back scatter image, and **c** EDS elemental analysis selection

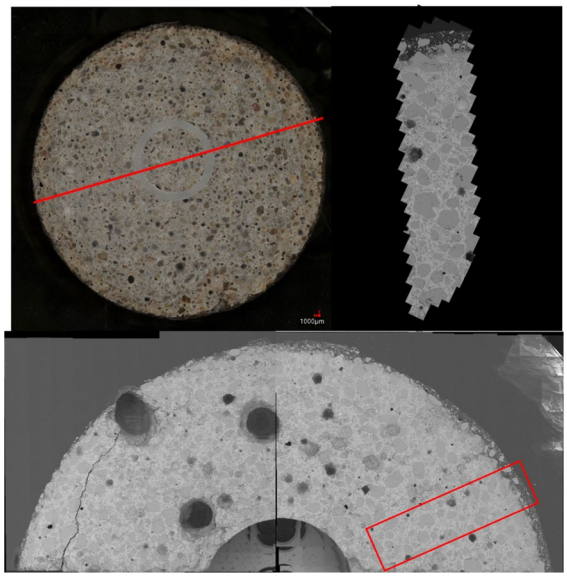

Fig. 11 Analysis of CEM II mortar: cross section visualization with Keyence, SEM imaging, and EDS elemental analysis selection

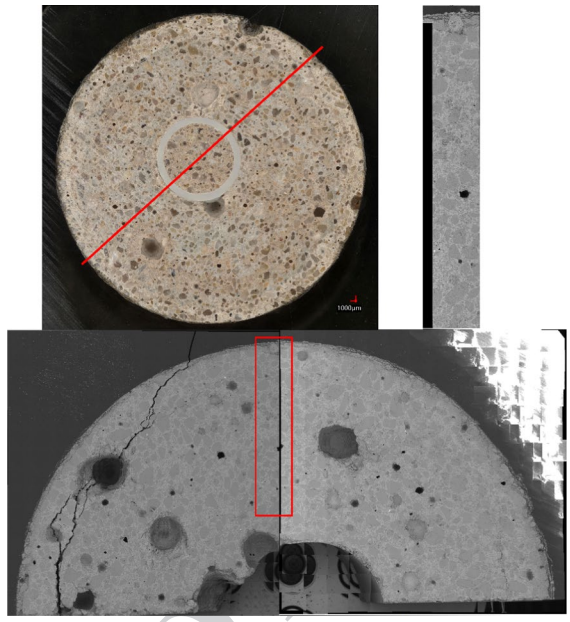

Fig. 12 Analysis of CEM III mortar: Cross section visualization with Keyence, SEM imaging, and EDS elemental analysis selection

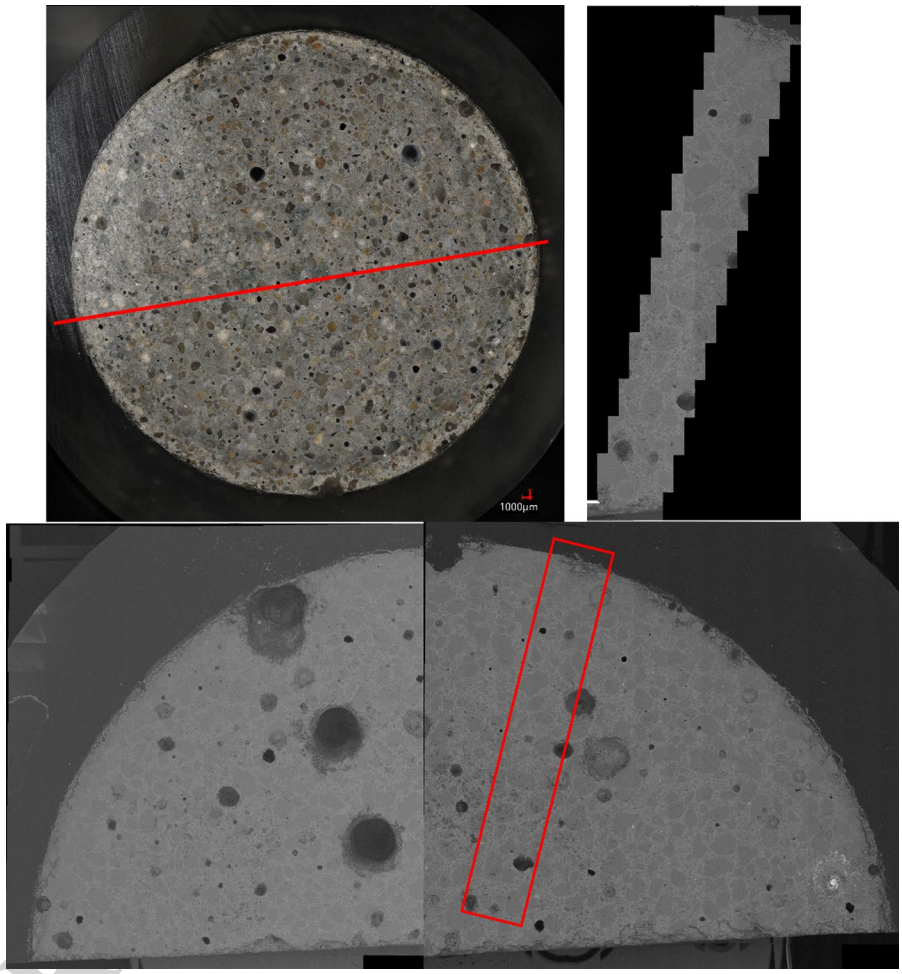

Fig. 13 Analysis of CEM V mortar: Cross section visualization with Keyence, SEM imaging, and EDS elemental analysis selection

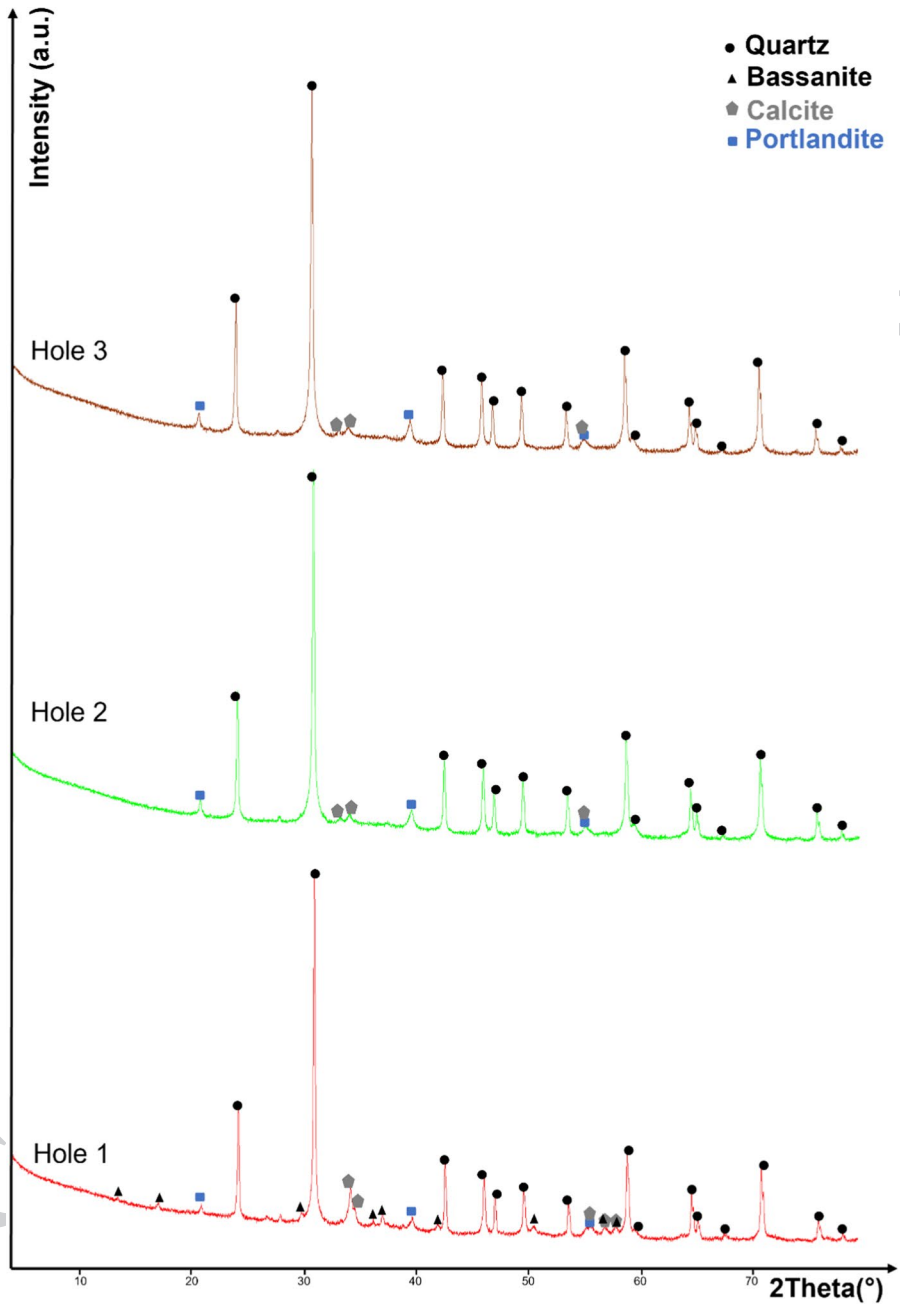

Fig. 14 RDX diagram of the three holes in the CEM I specimen

References

1. Kaempfer W, Berndt M (1999) Estimation of service life of concrete pipes in sewer networks. Durab Build Mater Compon 8:36–45
2. Monteny J, Vincke E, Beeldens A et al (2000) Chemical, microbiological, and in situ test methods for biogenic sulfuric acid corrosion of concrete. Cem Concr Res 30:623–634. https://doi.org/10.1016/S0008-8846(00)00219-2
3. O'Connell M, McNally C, Richardson MG (2010) Biochemical attack on concrete in wastewater applications: a state of the art review. Cement Concr Compos 32:479–485. https://doi.org/10.1016/j.cemconcomp.2010.05.001
4. Stokbro Jensen H (2009) Hydrogen sulfide induced concrete corrosion of sewer networks: Ph. D. dissertation. Section of environmental engineering, Aalborg University
5. Okabe S, Odagiri M, Ito T, Satoh H (2007) Succession of sulfur-oxidizing bacteria in the microbial community

on corroding concrete in sewer systems. Appl Environ Microbiol 73:971–980. https://doi.org/10.1128/AEM.02054-06
6. Melchers RE, Bond P (2009) Factors involved in the long term corrosion of concrete sewers
7. MaGD G-P, Bielefeldt A, Ovtchinnikov S et al (2010) Biogenic sulfuric acid attack on different types of commercially produced concrete sewer pipes. Cem Concr Res 40:293–301. https://doi.org/10.1016/j.cemconres.2009.10.002
8. Herisson J (2012) Biodétérioration des matériaux cimentaires dans les ouvrages d'assainissement: étude comparative du ciment d'aluminate de calcium et du ciment Portland
9. Grandclerc A (2017) Compréhension des mécanismes de biodétérioration des matériaux cimentaires dans les réseaux d'assainissement: étude expérimentale et modélisation
10. Grengg C, Mittermayr F, Ukrainczyk N et al (2018) Advances in concrete materials for sewer systems affected by microbial induced concrete corrosion: a review. Water Res 134:341–352. https://doi.org/10.1016/j.watres.2018.01.043
11. Aboulela A (2022) Study of the resistance to biodeterioration of innovative low-carbon cementitious materials for application in sewer networks
12. Herisson J, van Hullebusch ED, Moletta-Denat M et al (2013) Toward an accelerated biodeterioration test to understand the behavior of Portland and calcium aluminate cementitious materials in sewer networks. Int Biodeterior Biodegradation 84:236–243. https://doi.org/10.1016/j.ibiod.2012.03.007
13. Wu M, Wang T, Wu K, Kan L (2020) Microbiologically induced corrosion of concrete in sewer structures: a review of the mechanisms and phenomena. Constr Build Mater 239:117813. https://doi.org/10.1016/j.conbuildmat.2019.117813
14. Haque F, Santos RM, Chiang YW (2019) Using nondestructive techniques in mineral carbonation for understanding reaction fundamentals. Powder Technol 357:134–148. https://doi.org/10.1016/j.powtec.2019.08.089
15. Potgieter-Vermaak SS, Potgieter JH, Van Grieken R (2006) The application of Raman spectrometry to investigate and characterize cement, Part I: a review. Cem Concr Res 36:656–662. https://doi.org/10.1016/j.cemconres.2005.09.008
16. Black L (2009) Raman spectroscopy of cementitious materials. In: Yarwood J, Douthwaite R, Duckett S (eds) Spectroscopic properties of inorganic and organometallic compounds. Royal Society of Chemistry, Cambridge, pp 72–127
17. Prieto-Taboada N, Larrañaga A, Gómez-Laserna O et al (2015) The relevance of the combination of XRD and Raman spectroscopy for the characterization of the CaSO4–H2O system compounds. Microchem J 122:102–109. https://doi.org/10.1016/j.microc.2015.04.010
18. Marchetti M, Mechling J-M, Janvier-Badosa S, Offroy M (2023) Benefits of chemometric and Raman spectroscopy applied to the kinetics of setting and early age hydration of cement paste. Appl Spectrosc 77:37–52. https://doi.org/10.1177/00037028221135065
19. FD (2022) P18–011. In: Afnor editions. https://www.boutique.afnor.org/fr-fr/norme/fd-p18011/beton-definition-et-classification-des-environnements-chimiquement-agressif/fa204582/328696. Accessed 4 Dec 2023
20. Downs RT, Hall-Wallace M (2003) The American mineralogist crystal structure database. Am Mineral 88:247–250
21. Gražulis S, Chateigner D, Downs RT et al (2009) Crystallography open database – an open-access collection of crystal structures. J Appl Cryst 42:726–729. https://doi.org/10.1107/S0021889809016690
22. Gražulis S, Daškevič A, Merkys A et al (2012) Crystallography open database (COD): an open-access collection of crystal structures and platform for world-wide collaboration. Nucleic Acids Res 40:D420–D427. https://doi.org/10.1093/nar/gkr900
23. Gražulis S, Merkys A, Vaitkus A, Okulič-Kazarinas M (2015) Computing stoichiometric molecular composition from crystal structures. J Appl Cryst 48:85–91. https://doi.org/10.1107/S1600576714025904
24. Merkys A, Vaitkus A, Butkus J et al (2016) COD::CIF::parser: an error-correcting CIF parser for the Perl language. J Appl Cryst 49:292–301. https://doi.org/10.1107/S1600576715022396
25. Quirós M, Gražulis S, Girdzijauskaitė S et al (2018) Using smiles strings for the description of chemical connectivity in the crystallography open database. J Cheminform 10:23. https://doi.org/10.1186/s13321-018-0279-6
26. Vaitkus A, Merkys A, Gražulis S (2021) Validation of the crystallography open database using the crystallographic information framework. J Appl Cryst 54:661–672. https://doi.org/10.1107/S1600576720016532
27. Merkys A, Vaitkus A, Grybauskas A et al (2023) Graph isomorphism-based algorithm for cross-checking chemical and crystallographic descriptions. J Cheminform 15:25. https://doi.org/10.1186/s13321-023-00692-1
28. Gutierrez RMP (2017) Chapter 2 - A novel approach to the oral delivery of bionanostructures for systemic disease
29. Tang C, Ling T-C, Mo KH (2021) Raman spectroscopy as a tool to understand the mechanism of concrete durability—a review. Constr Build Mater 268:121079. https://doi.org/10.1016/j.conbuildmat.2020.121079
30. Herisson J, Guéguen-Minerbe M, Van Hullebusch ED, Chaussadent T (2014) Behaviour of different cementitious material formulations in sewer networks. Water Sci Technol 69:1502–1508. https://doi.org/10.2166/wst.2014.009
31. Herisson J, Guéguen-Minerbe M, Van Hullebusch ED, Chaussadent T (2017) Influence of the binder on the behaviour of mortars exposed to H2S in sewer networks: a long-term durability study. Mater Struct 50:8. https://doi.org/10.1617/s11527-016-0919-0
32. Pons T, Gueguen M, Grandclerc A et al (2018) Field investigation of cementitious materials durability in sewer environment
33. Grengg C, Mittermayr F, Koraimann G et al (2017) The decisive role of acidophilic bacteria in concrete sewer networks: a new model for fast progressing microbial

concrete corrosion. Cem Concr Res 101:93–101. https://doi.org/10.1016/j.cemconres.2017.08.020
34. Grengg C, Ukrainczyk N, Koraimann G et al (2020) Long-term in situ performance of geopolymer, calcium aluminate and Portland cement-based materials exposed to microbially induced acid corrosion. Cem Concr Res 131:106034. https://doi.org/10.1016/j.cemconres.2020.106034
35. Grengg C, Koraimann G, Ukrainczyk N et al (2021) Cu- and Zn-doped alkali activated mortar – properties and durability in (bio)chemically aggressive wastewater environments. Cem Concr Res 149:106541. https://doi.org/10.1016/j.cemconres.2021.106541
36. Schneider CA, Rasband WS, Eliceiri KW (2012) NIH Image to ImageJ: 25 years of image analysis. Nat Methods 9:671–675. https://doi.org/10.1038/nmeth.2089
37. Pons T, Fourdrin C, Grandclerc A et al (2018) Mineralogical characterization of the alteration layer of chemically and biologically altered cementitious materials
38. Chukanov NV, Vigasina MF (2020) Vibrational (infrared and Raman) spectra of minerals and related compounds. Springer International Publishing, Cham
39. Bensted J (1976) Uses of Raman spectroscopy in cement chemistry. J Am Ceram Soc 59:140–143. https://doi.org/10.1111/j.1151-2916.1976.tb09451.x
40. Chang H, Huang PJ, Hou SC (1999) Application of thermo-Raman spectroscopy to study dehydration of CaSO4.2H2O and CaSO4.0.5H2O. Mater Chem Phys 58(1):12–19
41. Black L, Breen C, Yarwood J et al (2006) Hydration of tricalcium aluminate (C3A) in the presence and absence of gypsum—studied by Raman spectroscopy and X-ray diffraction. J Mater Chem 16:1263. https://doi.org/10.1039/b509904h
42. Black L, Breen C, Yarwood J et al (2007) Structural features of C-S–H(I) and Its carbonation in air—a Raman spectroscopic study. Part II: carbonated phases. J Am Ceram Soc 90:908–917. https://doi.org/10.1111/j.1551-2916.2006.01429.x
43. Chollet M, Horgnies M (2011) Analyses of the surfaces of concrete by Raman and FT-IR spectroscopies: comparative study of hardened samples after demoulding and after organic post-treatment. Surf Interface Anal 43:714–725. https://doi.org/10.1002/sia.3548
44. Irassar EF, Bonavetti VL, González M (2003) Microstructural study of sulfate attack on ordinary and limestone Portland cements at ambient temperature. Cem Concr Res 33:31–41. https://doi.org/10.1016/S0008-8846(02)00914-6
45. Frost RL, Keeffe EC (2009) Raman spectroscopic study of the sulfite-bearing minerals scotlandite, hannebachite and orschallite: implications for the desulfation of soils. J Raman Spectrosc 40:244–248. https://doi.org/10.1002/jrs.2089
46. Scrivener KL, Crumbie AK, Laugesen P (2004) the interfacial transition zone (ITZ) between cement paste and aggregate in concrete. Interface Sci 12:411–421. https://doi.org/10.1023/B:INTS.0000042339.92990.4c
47. Mittermayr F, Rezvani M, Baldermann A et al (2015) Sulfate resistance of cement-reduced eco-friendly concretes. Cement Concr Compos 55:364–373. https://doi.org/10.1016/j.cemconcomp.2014.09.020
48. Appelo CAJ, Postma D (2004) Geochemistry, groundwater and pollution. CRC Press, Boca Raton
49. Grengg C, Gluth GJG, Mittermayr F et al (2021) Deterioration mechanism of alkali-activated materials in sulfuric acid and the influence of Cu: a micro-to-nano structural, elemental and stable isotopic multi-proxy study. Cem Concr Res 142:106373. https://doi.org/10.1016/j.cemconres.2021.106373

Journal:	**11527**
Article:	**2346**

Author Query Form

Please ensure you fill out your response to the queries raised below and return this form along with your corrections

Dear Author

During the process of typesetting your article, the following queries have arisen. Please check your typeset proof carefully against the queries listed below and mark the necessary changes either directly on the proof/online grid or in the 'Author's response' area provided below

Query	Details Required	Author's Response
AQ1	Please confirm if the author names are presented accurately and in the correct sequence (given name, middle name/initial, family name). Author 2 Given name: [Marielle Guéguen] Last name [Minerbe]. Also, kindly confirm the details in the metadata are correct.	
AQ2	Journal instruction requires a city for affiliations; however, these are missing in affiliation [1, 3]. Please verify if the provided city are correct and amend if necessary.	
AQ3	Please check and confirm the Figure 2 has changed to Figure 1, Figure3 has changed to Figure 2, Figure 1 has changed to Figure 3 are arranged in correct sequences.	
AQ4	Please check and confirm the inserted Table 2 is correctly identified.	
AQ5	Please check and confirm the Table 1 caption has changed to Table 2 is correctly identified.	